Research Square

Preprints are preliminary reports that have not undergone peer review.
They should not be considered conclusive, used to inform clinical practice,
or referenced by the media as validated information.

Time-dependent dragload and neutral plane of a pile beneath an approach embankment on stratified clay: unified method versus coupled consolidation analysis

Henrry Bazán

henrry.villanueva@upn.edu.pe

UNIVERSIDAD PRIVADA DEL NORTE

Research Article

Keywords: Negative skin friction, Dragload, Neutral plane, Approach embankment, Consolidation, Finite element analysis

Posted Date: November 3rd, 2026

DOI: https://doi.org/10.21203/rs.3.rs-11422365/v1

License: This work is licensed under a Creative Commons Attribution 4.0 International License.
Read Full License

Additional Declarations: No competing interests reported.

Time-dependent dragload and neutral plane of a pile beneath an approach embankment on stratified clay: unified method versus coupled consolidation analysis

Abstract

Purpose Piles built before an approach embankment on compressible clay are dragged down as the clay consolidates. The unified method gives the long-term dragload and neutral plane from an assumed toe stiffness and fully mobilised shaft shear, and says nothing about time. This study measures what those assumptions cost for a pile through high-plasticity clay over low-plasticity clay.

Methods A 0.6 m by 18 m pile carrying 600 kN beneath a 3 m embankment (54 kPa) was analysed with the unified method and with a coupled finite-element consolidation model with a frictional interface. The clay was modelled as equivalent elastic and as Modified Cam Clay, with consolidation followed for 600 years. The model was checked against an independent one-dimensional solution and four meshes; twelve variations were run.

Results Final dragload was 444 kN with Modified Cam Clay and 459 kN with elastic clay, against 801 kN from the unified method; the neutral plane lay at 12.6 and 13.5 m instead of 14.25 m. About 166 kN of the gap came from toe stiffness and 180 kN from partial mobilisation over a 9 m transition zone. Dragload lagged settlement: at 34% consolidation the pile carried 19% of its final dragload. With a draining bearing stratum, 61% arrived within the first year.

Conclusion With inputs consistent with the model, the rigid-plastic method located the neutral plane within about 0.2 m but overestimated the dragload by 32 to 41%. Toe response and drainage of the bearing stratum controlled magnitude and timing more than interface strength did.

Keywords Negative skin friction · Dragload · Neutral plane · Approach embankment · Consolidation · Finite element analysis

1 Introduction

Bridge abutments, wing walls, culverts and sign structures are often founded on piles that are installed before, or together with, the approach embankment. Where the subsoil is compressible clay, the fill makes the ground settle for years while the piles, supported at depth, barely move. The soil then hangs on the shaft. The resulting negative skin friction adds an axial force to the pile, the dragload, and pulls the pile down with the ground, the downdrag.

The phenomenon was measured early on highway works. Bozozuk [1] instrumented a 49 m steel pipe pile driven beneath a 9 m granular embankment on a Quebec motorway: the fill settled 53 cm and the pile developed a peak load of 140 t at 22 m below its head. Fellenius [2] measured the dragload that built up on instrumented piles driven through soft clay, and Indraratna et al. [3] followed driven piles under embankment loading in soft Bangkok clay, where an effective-stress approach with β between 0.1 and 0.2 reproduced the measured friction. Long-term records from several countries show that load transfer is governed by effective stress and that very

small relative movements are enough to mobilise the shaft shear [4]. More recent case histories keep coming from transportation projects: settlement of a bridge abutment and its approach attributed to downdrag on timber piles [5], differential movement at embankment–structure interfaces [6], and drag forces induced on piles by the construction of a bridge embankment [7]. Model and field tests have also examined how a pile under negative skin friction responds to axial load [8-10].

For design, the dragload and the neutral plane are usually obtained with the unified method [11], which has been taken up in recent highway research and guidance [12]. The method balances forces along the pile and looks for the depth at which pile and soil settle equally. Above that depth the shaft shear is taken as fully mobilised downward, below it as fully mobilised upward. Poulos [13] proposed a practical approach that designs the part of the pile located in the stable ground below the settling layers. Simplified analyses have dealt with the transfer mechanism, the neutral plane and layered deposits [14-16], and load-transfer models coupled with consolidation theory predict how the friction grows [17-19].

Numerical work points to the interface as the decisive element. Lee et al. [20] found that slip at the pile–soil interface was the most important factor in consolidating ground and that existing design approaches overpredicted the dragload of single piles. Later analyses examined slip [21], pile groups [22, 23], surcharge loading of single piles in clay [24], the combined influence of consolidation and pile-head load [25, 26], fully coupled consolidation [27, 28], effective-stress and finite-element estimates for a single pile [29] and installation effects [30]. Related work in this journal has reported experimental studies of negative skin friction on single and grouped piles [31, 32], the long-term consolidation settlement of piled foundations on soft clay [33], the deformation of bridge–embankment transition zones on soft soil [34] and the time-dependent behaviour of geosynthetic-reinforced pile-supported embankments [35].

The problem lies in how that method is used in practice. A designer who applies it to a stratified profile has to make three choices that the method itself does not resolve. The toe stiffness is assumed, because a loading test with toe instrumentation is rarely available when the piles of an approach are designed. The shaft shear is taken as fully mobilised on both sides of the neutral plane, although the relative movement near that plane is, by definition, close to zero. And the result is a long-term state, with no indication of whether the dragload arrives in the first year of the embankment or decades later. The three choices weigh on different parts of the design. The first two fix how much dragload enters the structural check of the section and where the neutral plane falls, which governs the settlement of the pile. The third decides, at a bridge approach, whether the dragload acts together with the early settlement of the structure or long after, with the abutment already in service. Numerical analyses have shown that the rigid-plastic simplification overpredicts the dragload of single piles [20, 21], but they do not say how much of the difference belongs to each assumption, nor how the dragload develops in time in a stratified profile.

The recent literature does not close that gap either. Coupled models have shown the role of interface slip [21] and of the head load [25, 26], and load-transfer models coupled with consolidation follow the growth of the friction in time [17-19]. None of them separates, for one case, the part of the difference with the unified method that comes from the assumed toe stiffness from the part that comes from partial mobilisation, or relates the progress of the dragload to the degree of consolidation, which is what a settlement record under the embankment

can measure. The work on these topics published in this journal deals with collapsible gypseous soil in physical models, with piled rafts and with reinforced piled embankments. No paper in the journal has yet examined a pile dragged by consolidating clay beneath an approach embankment, with a bearing stratum that may or may not drain.

This paper takes that case in one specific version: a bored pile beneath an approach embankment on a high-plasticity clay overlying a low-plasticity clay. The same case is solved with the unified method and with a coupled consolidation model with a frictional interface, using the same soil parameters, so that what differs between the two results is the method and not the input. The objectives are (1) to compare the two calculations at the end of consolidation, (2) to separate the part of the difference caused by the assumed toe stiffness from the part caused by partial mobilisation, (3) to follow dragload and neutral plane through time and relate them to the degree of consolidation, including the effect of drainage of the bearing stratum, and (4) to rank the influence of interface strength, toe stiffness, head load and interface stiffness. What the paper offers design is an answer to the three choices above: how much the result changes when the toe stiffness is measured instead of assumed; by how much the rigid-plastic method overestimates the dragload, and how well it locates the neutral plane, once its inputs are consistent; and which property of the ground, the drainage of the bearing stratum, decides whether the dragload arrives within a year or over decades. With those answers the unified method can still be used, but with its assumptions bounded. The case is parametric. Its soil parameters are illustrative and are not tied to a site, so the results show mechanisms and orders of magnitude and should not be read as the design of any project.

2 Problem definition

The case is shown in Fig. 1a. A cast-in-place concrete pile, 0.60 m in diameter and 18 m long, with a Young's modulus of 30 GPa, carries a sustained head load of 600 kN. It is installed before a 3 m embankment with a unit weight of 18 kN/m³ is placed, which adds 54 kPa at the ground surface. The head load stands for the sustained reaction of a structure founded at the original ground level, such as a culvert or an abutment footing. The slenderness ratio is 30.

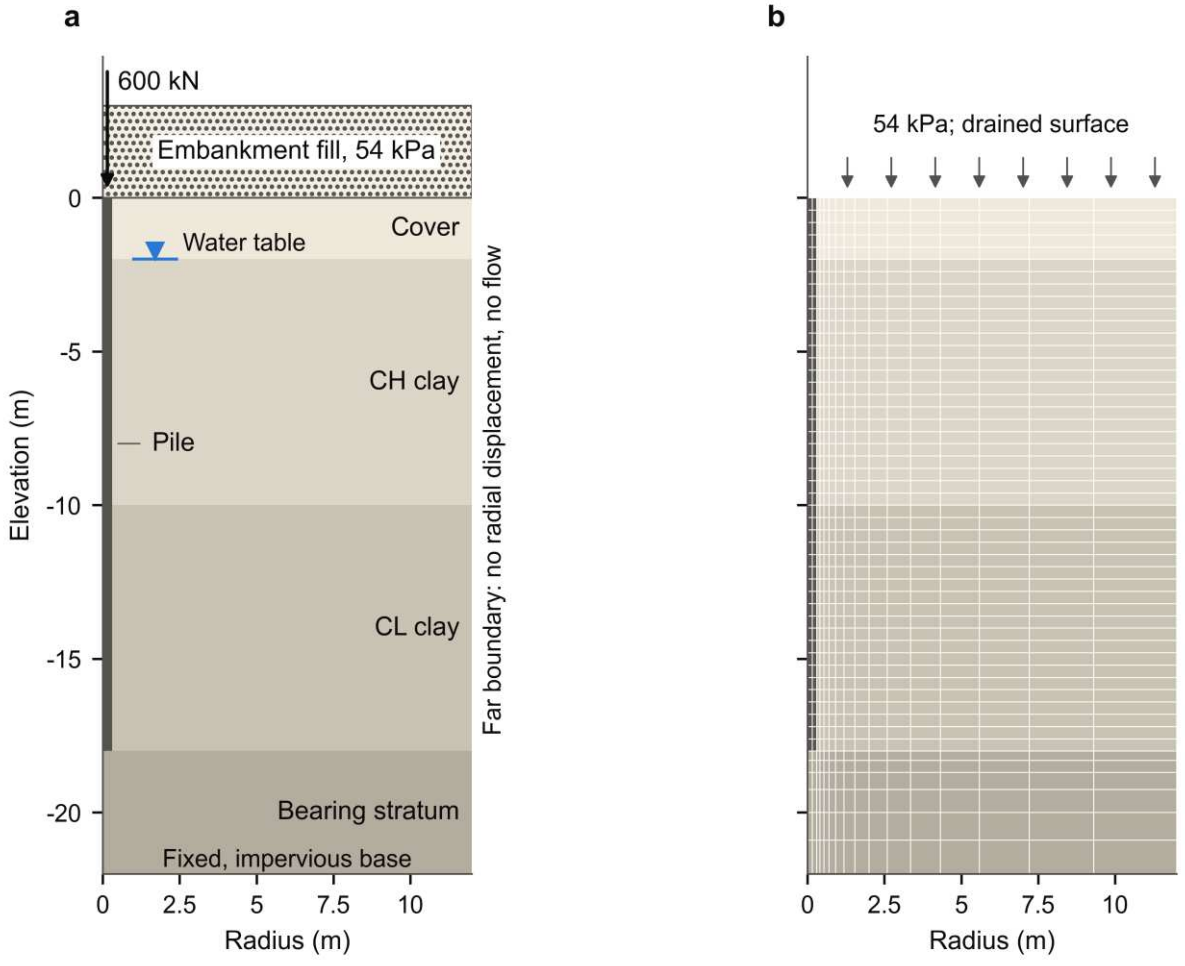
The ground consists of a 2 m cover above the water table, 8 m of high-plasticity clay (CH), 8 m of low-plasticity clay (CL) and a stiffer bearing stratum in which the pile toe rests at 18 m. The water table is at the top of the CH layer. Table 1 lists the parameters. The compression and recompression indices, initial void ratios, overconsolidation ratios (OCR) and friction angles of the two clays are the same in both methods, so that the comparison is not affected by parameter choice. The friction angle of the CH layer is at the low end for such soils; its influence enters through the interface coefficient and is examined in the parametric study.

The embankment is taken as wide compared with the 16 m of compressible clay, so the surcharge is uniform and the far-field compression is one-dimensional. This suits a pile inside the footprint of the embankment and away from the toe of its slope. Lateral soil movement near the slope, which bends abutment piles, is outside the scope.

106 **Table 1** Soil and interface parameters of the case

Parameter	Cover	CH clay	CL clay	Bearing stratum
Depth (m)	0–2	2–10	10–18	18–22
Unit weight (kN/m³)[a]	18.0	17.5	19.0	20.0
Initial void ratio, e_0	0.60	1.10	0.72	0.50
Compression index, C_c	–	0.42	0.20	–
Recompression index, C_r	–	0.060	0.035	–
Overconsolidation ratio, OCR	–	1.2	1.5	–
Friction angle, φ' (°)	–	14	22	–
Earth pressure coefficient at rest, K_0	0.50	0.83	0.77	0.45
Permeability, k (m/s)	5×10^{-8}	1×10^{-10}	1×10^{-9}	1×10^{-8}
Young's modulus, E (kPa)	8000	997[b]	12 756[b]	60 000
Poisson's ratio, ν	0.30	0.30	0.30	0.28
Cam Clay λ	–	0.182	0.087	–
Cam Clay κ	–	0.026	0.015	–
Cam Clay M	–	0.526	0.856	–
Interface coefficient, μ	0	0.249	0.404	–

107 [a] Total unit weight in the cover, which lies above the water table; saturated unit weight in the other layers. [b]
108 Equivalent elastic model, Eq. (11)



109

110 **Fig. 1** Case analysed: **a** stratigraphy, pile and loading; **b** finite-element mesh of the axisymmetric model (932
111 nodes)

3 Methods

3.1 Unified method

The unified method was applied in its rigid-plastic form [11]. Depth z is measured from the pile head. The compressible profile was divided into 0.05 m segments. Both clays are overconsolidated, with a preconsolidation stress $\sigma'_p = \mathrm{OCR}\,\sigma'_{v0}$. The surcharge takes the CH layer and the top metre of the CL layer past that stress, and leaves the rest of the CL layer below it. Where it is exceeded, the vertical strain of a segment follows the usual compression-index relation [36], Eq. (1):

$$\varepsilon_v = \frac{C_r \log_{10}\left(\sigma'_p/\sigma'_{v0}\right) + C_c \log_{10}\left(\sigma'_{vf}/\sigma'_p\right)}{1 + e_0} \qquad (1)$$

where σ'_{v0} and σ'_{vf} are the initial and final vertical effective stresses, C_c and C_r the compression and recompression indices and e_0 the initial void ratio. Where σ'_{vf} stays below σ'_p the strain reduces to $C_r \log_{10}(\sigma'_{vf}/\sigma'_{v0})/(1 + e_0)$. The settlement of the soil at depth z is the compression accumulated between that depth and the base of the compressible profile, z_b = 18 m, as written in Eq. (2):

$$s_s(z) = \int_z^{z_b} \varepsilon_v \, \mathrm{d}z \qquad (2)$$

The unit shaft resistance r_s was computed with the effective-stress (β) method [37], Eq. (3). The coefficient of earth pressure at rest takes the square-root form that Meyerhof used for overconsolidated clay. Mayne and Kulhawy [38] later proposed the exponent $\sin\varphi'$ in place of 0.5, which would lower β by about 5% in both clays. The square-root form is kept; Sect. 4.4 compares the shaft resistance it gives with the interface strength that the coupled model develops:

$$r_s = \beta\, \sigma'_{vf}, \qquad \beta = K_0 \tan\delta, \qquad K_0 = (1 - \sin\varphi')\mathrm{OCR}^{0.5} \qquad (3)$$

Here δ is the interface friction angle, taken equal to the friction angle φ' in the base case. Equation (3) gives β = 0.207 for the CH layer and 0.309 for the CL layer. No shaft resistance was assigned to the cover.

Above the neutral plane, at depth z_n, the soil moves down relative to the pile and r_s adds to the axial force. Below it the pile moves down relative to the soil and r_s is subtracted. With P the head load and D the diameter, the axial force Q is given by Eq. (4):

$$Q(z) = P + \pi D \int_0^z r_s \, \mathrm{d}z \quad (z \le z_n), \qquad Q(z) = Q(z_n) - \pi D \int_{z_n}^z r_s \, \mathrm{d}z \quad (z > z_n) \qquad (4)$$

The toe is a linear spring, Eq. (5). Its stiffness k_t was set at 100 MN/m, an assumed value of the kind used when no loading test is available:

$$R_t = Q(L) = k_t\, w_t \qquad (5)$$

where R_t is the toe load, L the pile length and w_t the toe settlement. The neutral plane is the depth at which the settlement of the soil, Eq. (2), equals that of the pile, which is the toe settlement plus the shortening of the pile below that depth. This condition is Eq. (6):

$$s_s(z_n) = w_t + \int_{z_n}^{L} \frac{Q}{E_p A_p}\,\mathrm{d}z \qquad (6)$$

where $E_p A_p$ is the axial rigidity of the pile. Equations (4) to (6) were solved by trying every segment boundary as the neutral plane and keeping the one with the smallest mismatch in Eq. (6). The dragload Q_d and the head settlement w_h then follow from Eq. (7):

$$Q_d = Q(z_n) - P, \qquad w_h = w_t + \int_0^{L} \frac{Q}{E_p A_p}\,\mathrm{d}z \qquad (7)$$

The calculation with k_t = 100 MN/m and the β values of Eq. (3) is called the reference calculation in what follows. Section 4.4 repeats it with inputs taken from the coupled model.

3.2 Coupled finite-element model

The same case was analysed with a coupled displacement–pore pressure formulation in Abaqus/Standard 2026 (Dassault Systèmes). The Learning Edition of the program was used, which limits a model to 1000 nodes. The model solves the equilibrium of the soil skeleton together with the continuity of the pore water, as in Biot's theory [39]. Both conditions are written in Eq. (8):

$$\nabla \cdot (\boldsymbol{\sigma}' - u\,\boldsymbol{I}) + \boldsymbol{\gamma}' = \mathbf{0}, \qquad \frac{\partial \varepsilon_{\mathrm{vol}}}{\partial t} + \frac{n}{K_w}\frac{\partial u}{\partial t} = \nabla \cdot \left(\frac{k}{\gamma_w}\nabla u\right) \qquad (8)$$

where $\boldsymbol{\sigma}'$ is the effective stress, positive in tension, u the excess pore pressure, $\boldsymbol{I}$ the unit tensor, $\boldsymbol{\gamma}'$ the effective unit weight, $\varepsilon_{\mathrm{vol}}$ the volumetric strain, n the porosity, K_w = 2.2 GPa the bulk modulus of water, k the permeability and γ_w the unit weight of water. Because u is the excess over hydrostatic, self-weight enters Eq. (8) as a body force with effective unit weights, total above the water table and submerged below it. The excess pore pressure is therefore zero before filling and returns to zero at the end.

The axisymmetric domain is 12 m in radius and 22 m deep (Fig. 1b). The soil is meshed with four-node elements with bilinear displacement and pore pressure, and the pile with four-node elements without pore pressure, in rows of 0.40 m along the shaft and 14 columns growing from 0.10 m at the pile to 2.8 m at the far boundary. The base mesh has 932 nodes. The ground surface is drained, with u = 0; the base and the far boundary are impervious in the base case. The far boundary is fixed radially and the base is fixed in both directions. Strains are small.

The pile is wished in place. The shaft interface is a single contact pair with Coulomb friction acting on the effective normal stress σ_n', which is the contact pressure less the pore pressure, as in earlier dragload analyses that allow slip [20, 21]. The shear stress τ is limited by Eq. (9):

$$|\tau| \le \mu\,\sigma_n', \qquad \mu = \tan\delta \qquad (9)$$

with μ = 0.249 in the CH layer and 0.404 in the CL layer, and no friction in the cover, as in the unified calculation. Sticking is enforced by a penalty stiffness that allows 2 mm of elastic slip before sliding. The toe bears on the stratum through frictionless contact. How much of the interface strength is in use at a given depth is expressed by the mobilisation ratio m of Eq. (10), where τ is positive when the soil drags the pile down:

$$m = \frac{\tau}{\mu\, \sigma_n'} \qquad (10)$$

so that $m = 1$ means fully mobilised negative skin friction and $m = -1$ fully mobilised positive resistance.

Four stages were run: geostatic equilibrium with a frictionless shaft; activation of shaft friction; application of the 600 kN head load under drained conditions; and placement of the 54 kPa surcharge on the ground surface around the pile over three months, followed by consolidation to 600 years, with results stored at 20 times. The pile head receives no load other than the 600 kN. Time steps were chosen automatically, with a limit of 3 kPa on the pore pressure change per increment.

Two descriptions of the clays were used. In the first, each clay is linear elastic. Its Young's modulus E is the one that reproduces the layer settlement of Eqs. (1) and (2), and it is obtained from the constrained modulus M_{oed} with Eq. (11):

$$E = M_{\mathrm{oed}}\, \frac{(1+\nu)(1-2\nu)}{1-\nu}, \qquad M_{\mathrm{oed}} = \frac{\Delta\sigma\, H}{s} \qquad (11)$$

where $\Delta\sigma$ is the surcharge, H the layer thickness, s its settlement and ν Poisson's ratio. Equation (11) gives 997 kPa for the CH layer and 12 756 kPa for the CL layer.

In the second description the clays follow Modified Cam Clay [36]. Its parameters come from the same indices and friction angle through Eq. (12):

$$\lambda = \frac{C_c}{\ln 10}, \qquad \kappa = \frac{C_r}{\ln 10}, \qquad M = \frac{6\sin\varphi'}{3-\sin\varphi'} \qquad (12)$$

The initial size of the yield surface was set so that the one-dimensional normal compression line of the model itself passes through σ_p'. In one-dimensional virgin compression the model settles at a stress ratio $\eta_K = q/p'$, where q is the deviator stress and p' the mean effective stress. That ratio follows from the flow rule of the model when the lateral strain is zero and elastic shear strains are neglected [36], and it fixes the at-rest coefficient of the model, $K_{0,\mathrm{nc}}$. Both are given by Eq. (13):

$$\eta_K^2 + 3\left(1-\frac{\kappa}{\lambda}\right)\eta_K - M^2 = 0, \qquad K_{0,\mathrm{nc}} = \frac{3-\eta_K}{3+2\eta_K} \qquad (13)$$

The preconsolidation pressure p_c' of the model is the size of the yield surface that passes through that stress state when the vertical stress is σ_p', Eq. (14):

$$p_c' = \sigma_p'\, \frac{1+2K_{0,\mathrm{nc}}}{3}\left(1+\frac{\eta_K^2}{M^2}\right) \qquad (14)$$

Because σ_p', and with it p_c', grows with depth, each row of elements received its own value. Placing the yield surface with Jaky's $K_{0,\mathrm{nc}} = 1 - \sin\varphi'$ [38] in Eq. (14) left the model stiffer than the oedometer curve of Eq. (1), and that variant is reported only as a sensitivity case. The cover and the bearing stratum are linear elastic in both models, and permeability is constant in each layer.

The axial force in the pile was obtained by integrating the vertical stress σ_{zz} over the pile section and subtracting the force Q_0 at the end of the geostatic stage, which balances the submerged weight of the pile. This is Eq. (15):

$$Q(z) = -\int_{A_p} \sigma_{zz}\, \mathrm{d}A - Q_0(z) \qquad (15)$$

The forces reported are therefore net of self-weight and can be compared with Eq. (4). The dragload was taken from them with Eq. (7), and the neutral plane was read as the depth at which the shaft shear, and with it the ratio of Eq. (10), changes sign.

3.3 Verification and parametric programme

Three checks were made. The first compared the far-field settlement of the elastic model with an independent solution of one-dimensional consolidation [40] for the layered column, under a surface load σ_s that grows to the full surcharge $\Delta\sigma$ during the three-month ramp. The equation solved and the settlement s that results are given in Eq. (16):

$$m_v \frac{\partial u}{\partial t} = \frac{\partial}{\partial z}\left(\frac{k}{\gamma_w}\frac{\partial u}{\partial z}\right) + m_v \frac{\mathrm{d}\sigma_s}{\mathrm{d}t}, \qquad s(t) = \int_0^{z_d} m_v\, (\sigma_s - u)\, \mathrm{d}z \qquad (16)$$

where $m_v = 1/M_{\mathrm{oed}}$ is the compressibility of each layer and z_d = 22 m the depth of the model. Equation (16) was solved in a separate program with implicit finite differences, the same layer moduli and permeabilities, a drained surface and an impervious base. The second check repeated the Modified Cam Clay case with three other meshes inside the node limit. The third compared the axial force of Eq. (15) with the force obtained by adding the integrated contact shear to the head load.

The time steps were also compared with the lower bound below which pore pressures oscillate in space [41]. For the backward-difference scheme used here that bound is Eq. (17):

$$\Delta t \geq \frac{(\Delta h)^2}{6\, c_v}, \qquad c_v = \frac{k\, M_{\mathrm{oed}}}{\gamma_w} \qquad (17)$$

where Δt is the time step, Δh the element size in the direction of flow and c_v the coefficient of consolidation. For the CH layer of the elastic model, with Δh = 0.40 m and c_v = 0.43 m²/year, the bound is 0.06 years.

Progress of consolidation is measured by the degree of consolidation U of Eq. (18), with s the far-field settlement of the ground surface and s_∞ its final value:

$$U(t) = \frac{s(t)}{s_\infty} \qquad (18)$$

Twelve variations of the Modified Cam Clay case were then run, one parameter at a time: interface factor tan δ / tan φ′ of 0.70 and 0.85, in the range usually measured between clay and concrete [42]; Young's modulus of the bearing stratum of 30, 120 and 240 MPa; head load of 300 and 900 kN; interface elastic slip of 1 and 5 mm; a drained base, which represents a pervious bearing stratum; clay permeability three times higher; and the Jaky-based placement of the yield surface.

4 Results

4.1 Verification

The elastic model reached a far-field surface settlement of 358.9 mm, against 359.9 mm from the independent solution of Eq. (16), and the largest difference along the whole curve was 3.3 mm, at 200 years (Fig. 2). The two clay layers settled 346.1 mm together, within 1 mm of the 347.1 mm given by Eqs. (1) and (2). The Modified Cam Clay model settled 362.7 mm at the top of the CH layer, 4.5% more.

During the three-month ramp the limit on pore pressure change forced steps of about 0.01 years, below the 0.06 years of Eq. (17). The result was a pore pressure overshoot in the row of nodes just below the drained top of the CH layer. At the end of the ramp the excess pore pressure there reached 58.4 kPa in the Modified Cam Clay model and 54.9 kPa in the elastic one, against the 54 kPa applied. Six months after the start of filling the maximum was below 54.6 kPa in both models.

The four meshes gave final dragloads between 441.5 and 447.1 kN and neutral planes between 12.61 and 12.66 m (Table 2). The spread in dragload is 1.3% of the base value. The node limit prevented a finer mesh. This is a sensitivity check; a formal convergence study was not possible. The two routes to the axial force differed by at most 2.5 kN along the shaft and by 10 kN in the row next to the toe, where stresses concentrate at the corner.

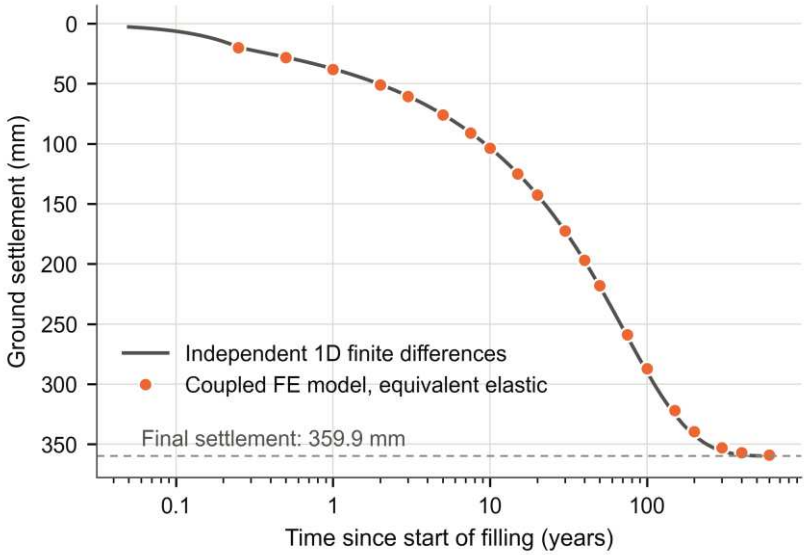


Fig. 2 Far-field ground settlement of the equivalent elastic model compared with an independent one-dimensional finite-difference solution

252 **Table 2** Mesh sensitivity of the Modified Cam Clay model at the end of consolidation

Mesh	Nodes	Dragload (kN)	Neutral plane (m)	Head settlement (mm)
Coarse: 0.50 m rows, 11 columns	641	447.1	12.66	16.23
Base: 0.40 m rows, 14 columns	932	443.6	12.63	16.31
Finer radially: 0.40 m rows, 15 columns	984	441.5	12.62	16.36
Finer vertically: 0.33 m rows, 12 columns	910	443.1	12.61	16.37

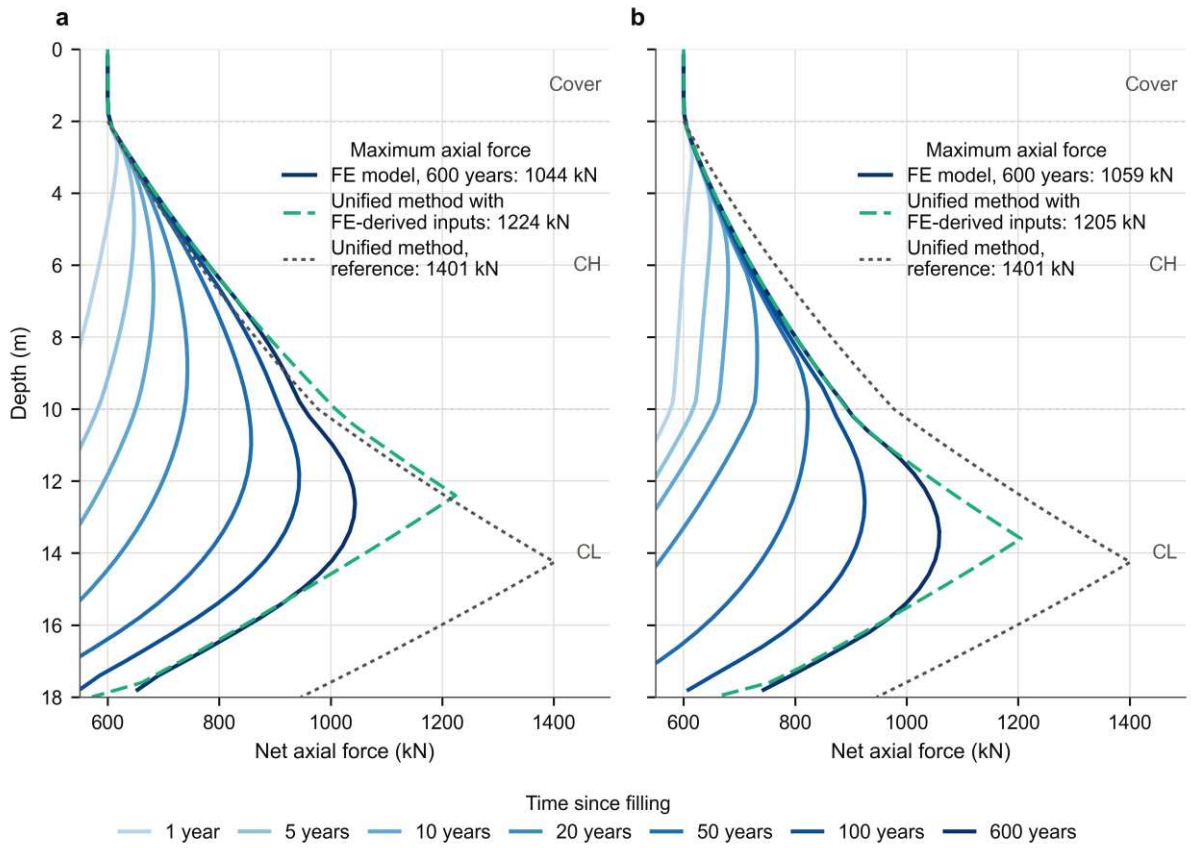
253 ## 4.2 State before filling

254 Under the 600 kN head load alone, the Modified Cam Clay model sent 412 kN to the shaft and 188 kN to the toe,
255 with a head settlement of 4.5 mm. The elastic model gave 364 kN, 236 kN and 5.6 mm. The shaft carried
256 positive resistance over its whole length, with a mobilisation ratio close to −0.5 in Eq. (10). This is the state that
257 the embankment later reverses in the upper part of the pile.

258 ## 4.3 End of consolidation

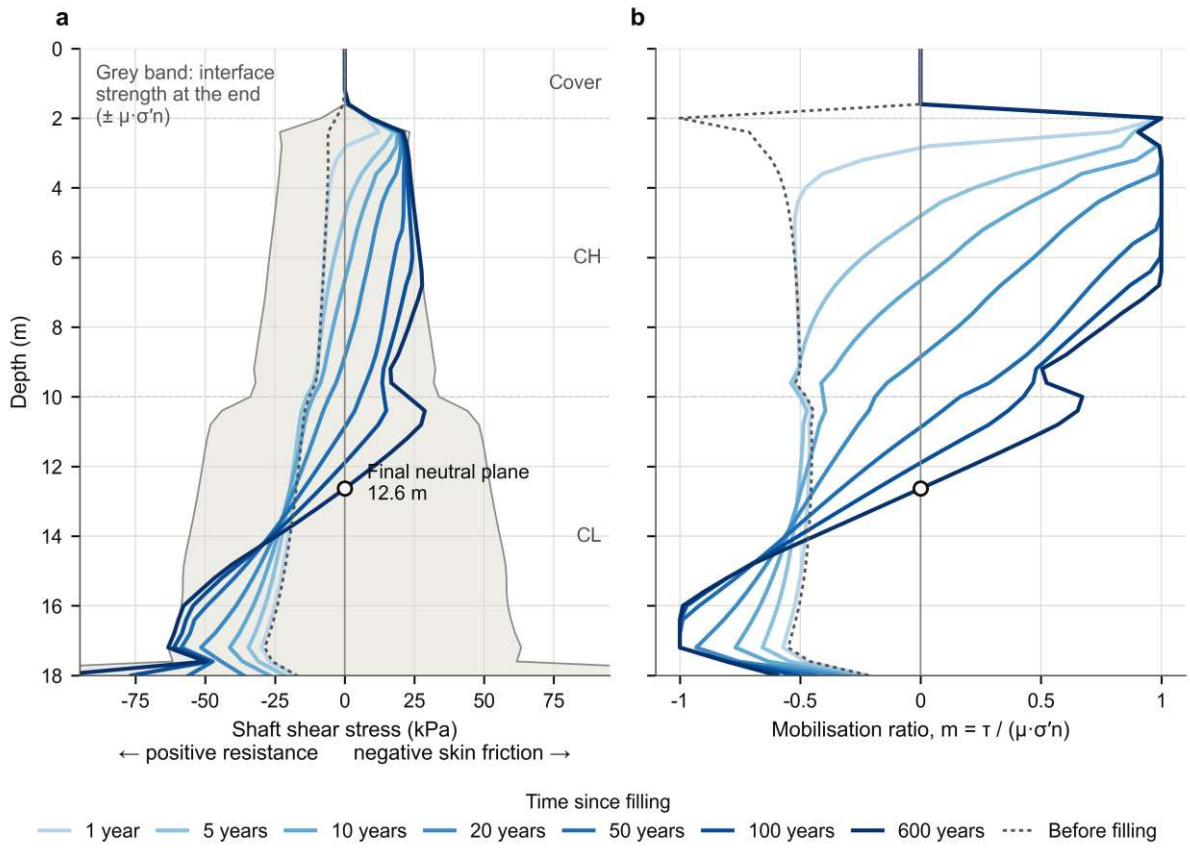
259 Table 3 compares the long-term results. The reference unified calculation, Eqs. (4) to (7), gave a dragload of 801
260 kN, a maximum axial force of 1401 kN and a neutral plane at 14.25 m. The coupled model gave 444 kN with
261 Modified Cam Clay and 459 kN with the elastic clay, and neutral planes at 12.63 and 13.51 m. The pile head
262 settled 16.3 and 17.7 mm in the two models, 11.8 and 12.1 mm of it after filling. The unified calculation gave
263 11.4 mm in total.

264 With Modified Cam Clay the axial force follows the unified method closely down to about 7 m and then falls
265 away from it (Fig. 3a). The reason is visible in the shaft shear (Fig. 4a) and in the mobilisation ratio of Eq. (10)
266 (Fig. 4b), where the dotted line is the state before filling. The interface is fully mobilised downward, with $m = 1$,
267 only from about 2.8 to 6.8 m. From there to 16 m the shear passes gradually from negative to positive, with a
268 small step at the boundary between the two clays, where the interface coefficient changes. It is fully mobilised
269 upward only between 16 and 17.2 m; in the two rows next to the toe the ratio falls back to −0.8 and −0.6, where
270 the corner disturbs the contact stresses. This transition zone is more than 9 m long, half the pile. It takes in the
271 lower part of the CH layer and nearly all of the CL layer, which is precisely where the unified method places its
272 largest shear. In the elastic model (Fig. 3b), whose shear is not plotted in Fig. 4, the transition is shorter and runs
273 from about 11 to 16.4 m.



274

275 **Fig. 3** Net axial force with depth at seven times after filling, with the two unified-method profiles for the final
276 state: **a** Modified Cam Clay; **b** equivalent elastic clay



277

278 **Fig. 4** Modified Cam Clay model: **a** shaft shear stress with depth, with the interface strength at the end of
279 consolidation; **b** mobilisation ratio of Eq. (10). The open circle marks the final neutral plane

280 **Table 3** Results at the end of consolidation

Calculation	Settlement at top of CH (mm)	Dragload (kN)	Maximum axial force (kN)	Neutral plane (m)	Head settlement (mm)
Unified method, reference calculation	347.1	801	1401	14.25	11.4
Unified method with the toe stiffness of the FE model	347.1	635	1235	12.70	16.0
Unified method with all inputs from the FE model, Modified Cam Clay	362.7	624	1224	12.40	15.0
Coupled FE model, Modified Cam Clay	362.7	444	1044	12.63	16.3
Unified method with all inputs from the FE model, equivalent elastic	348.9	605	1205	13.60	16.3
Coupled FE model, equivalent elastic	348.9	459	1059	13.51	17.7

281 ## 4.4 Sources of the difference

282 Two intermediate calculations split the 357 kN that lie between the reference calculation and the Modified Cam
283 Clay model.

284 The first replaces only the toe stiffness. At the end of consolidation the toe of the coupled model carried 631 kN
285 with a settlement of 14.6 mm. In Eq. (5) that is a secant stiffness of 43.3 MN/m, less than half the 100 MN/m
286 assumed. With that stiffness and nothing else changed, the unified method gives 635 kN and a neutral plane at
287 12.70 m. The toe accounts for 166 kN.

The second feeds the unified method with everything the coupled model can supply: its interface strength with depth, Eq. (9), its free-field settlement and its toe stiffness. The result is 624 kN and 12.40 m. The interface strength, where the two calculations might be expected to differ most, turned out to be nearly the same. Integrated over each layer, the interface strength of the coupled model is 406 kN in the CH layer against 377 kN from Eq. (3), because Modified Cam Clay develops a lateral stress coefficient of about 0.90 in normally consolidated compression where Eq. (3) uses 0.83, and 871 kN against 879 kN in the CL layer. These inputs move the dragload by only 11 kN.

The remaining 180 kN separate a rigid-plastic calculation and a coupled one that share the same inputs. They are the effect of partial mobilisation alone. With shared inputs the rigid-plastic method places the neutral plane 0.23 m above that of the coupled model and overestimates the dragload by 41%. The elastic model leads to the same reading with different numbers: 605 kN against 459 kN, 32% more, with the two neutral planes 0.09 m apart.

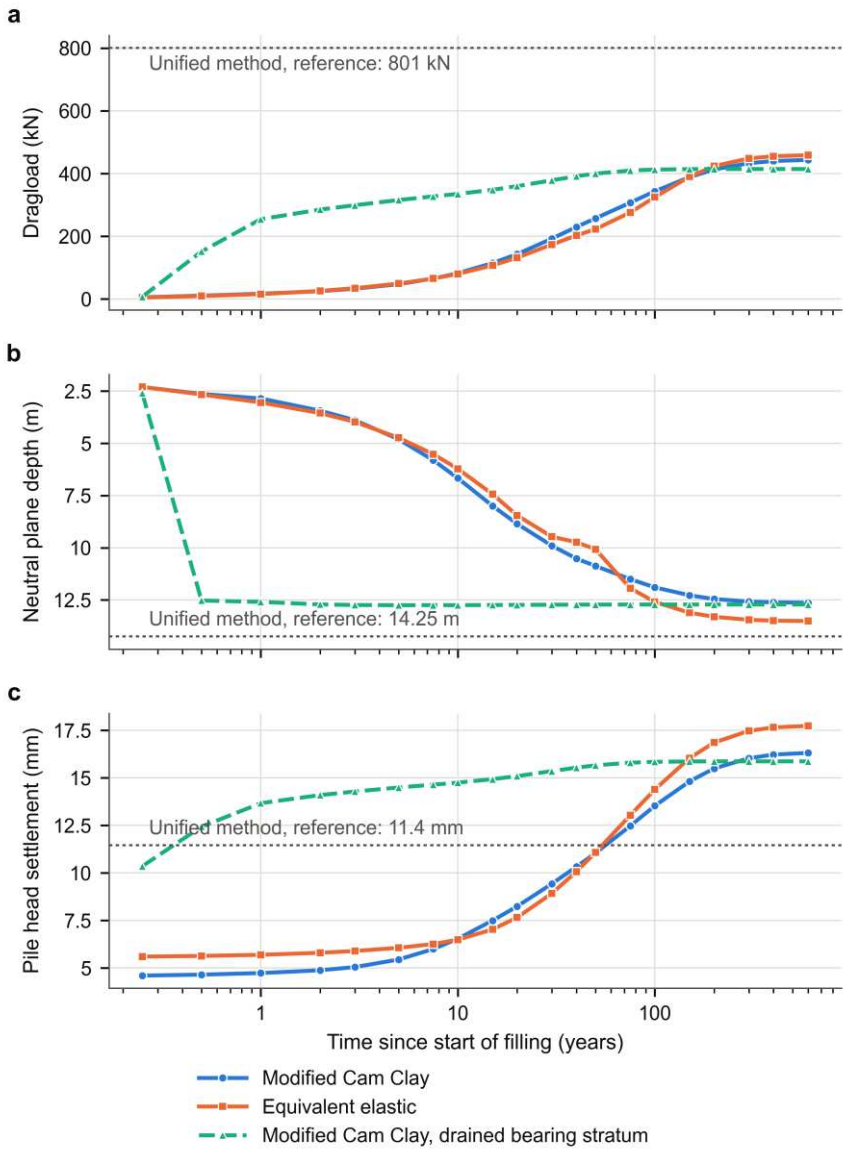
4.5 Development with time

Table 4 and Fig. 5 show the Modified Cam Clay results in time. One year after filling the ground had settled 48 mm, a degree of consolidation of 13% in Eq. (18), and the dragload was 17 kN. After 10 years the figures were 34% and 82 kN; after 50 years, 65% and 257 kN. Half of the final dragload was reached after 38 years and 90% after 171 years. The neutral plane moved down steadily, from 2.9 m at one year to 6.7 m at 10 years and 12.6 m at the end (Fig. 5b), as the consolidation front advanced from the drained surface. Chen et al. [25] described the same downward movement of the neutral plane with consolidation.

These absolute times follow directly from the permeability of 1×10^{-10} m/s adopted for the CH layer and from drainage towards the surface only. They are specific to the case. The relation between dragload and degree of consolidation is more general (Fig. 6). When the clay permeability was multiplied by three, the 90% time dropped to 59 years, but the points fell on the same curve. Along that curve the dragload lags the settlement: 19% of the final dragload at 34% consolidation and 58% at 65%. The elastic model behaved in the same way.

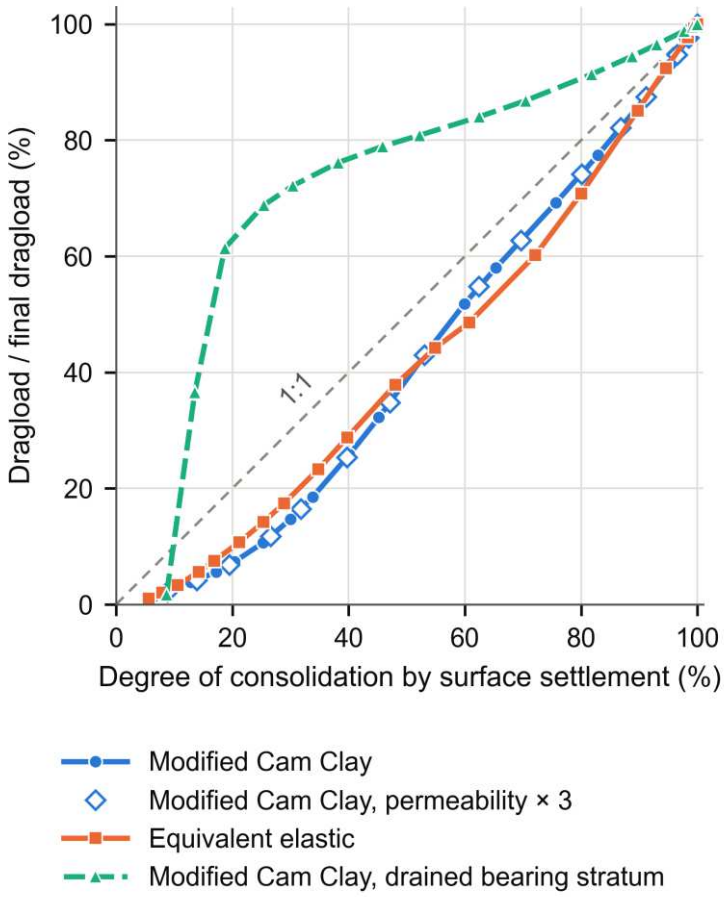
Drainage of the bearing stratum changed the picture. With a drained base the CL layer consolidated within months through the stratum below it, the neutral plane dropped to 12.5 m in half a year, and the dragload reached 254 kN, 61% of its final value, one year after filling, when the surface had settled only 19% (Figs. 5 and 6). Ninety per cent was reached in 27 years. The final dragload in this case was 414 kN, 7% lower than with the impervious base, because the interface response depends on the order in which the layers consolidate.

The excess pore pressure and settlement fields of the base case (Fig. 7) show the front moving down from the drained surface and the ground hanging on the pile. At the surface the soil next to the shaft settled 356 mm, against 373 mm in the free field.



319

320 **Fig. 5** Development with time of **a** dragload, **b** neutral plane depth and **c** pile head settlement. Dotted lines give
321 the long-term values of the reference unified calculation



322

323 **Fig. 6** Dragload as a fraction of its final value against the degree of consolidation of Eq. (18)

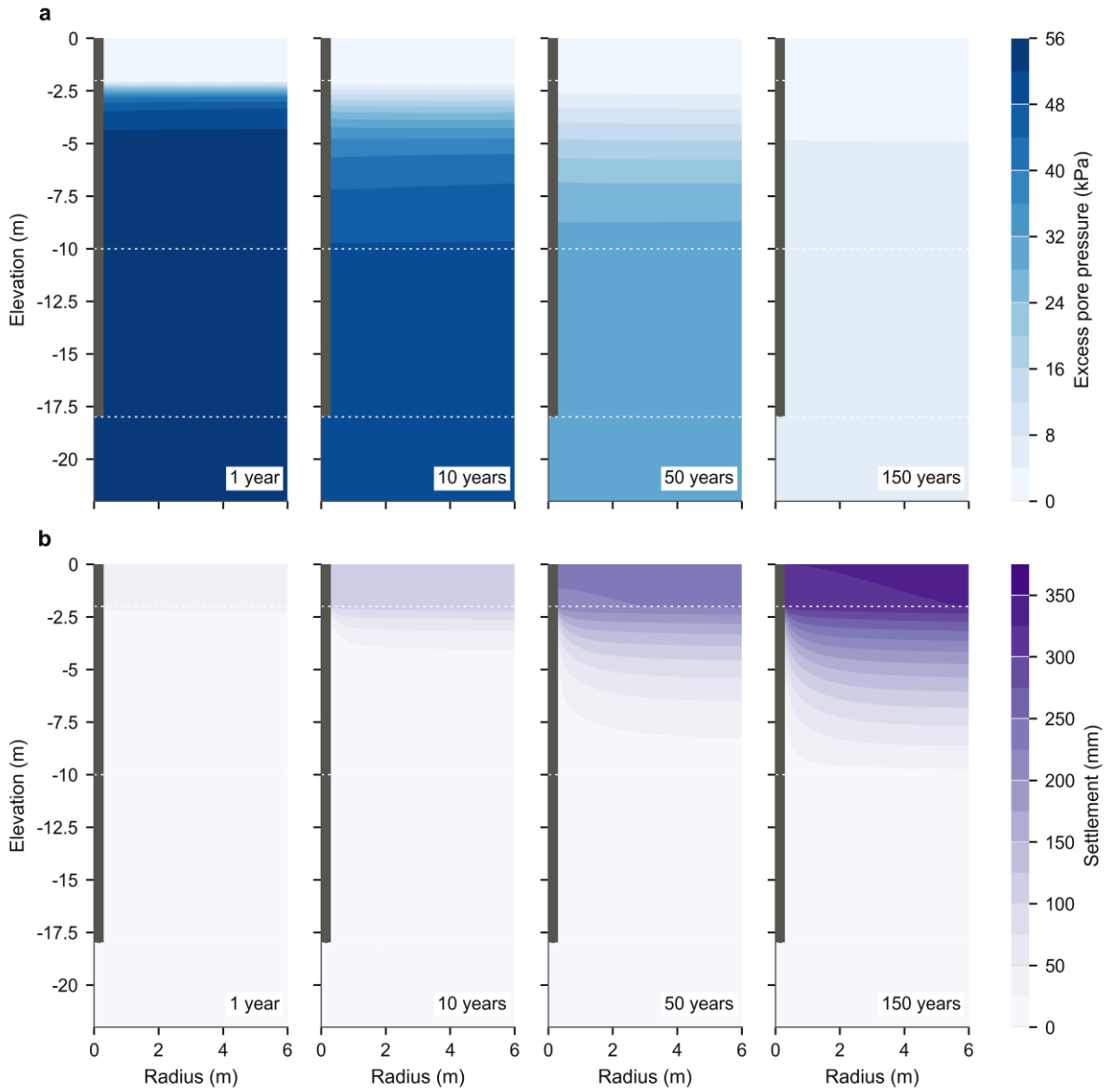


Fig. 7 Modified Cam Clay model at four times: **a** excess pore pressure; **b** settlement after filling. The grey strip is the pile and the dotted lines are the layer boundaries

Table 4 Development with time in the Modified Cam Clay model

Time (years)	Ground settlement (mm)	Degree of consolidation (%)	Dragload (kN)	Neutral plane (m)	Head settlement (mm)	Dragload with drained bearing stratum (kN)
1	47.9	13	17	2.9	4.7	254
5	94.1	25	47	4.8	5.4	316
10	126.0	34	82	6.7	6.5	335
20	168.4	45	143	8.9	8.2	360
50	243.4	65	257	10.9	11.0	400
100	308.9	83	344	11.9	13.5	413
200	355.5	95	413	12.5	15.5	414
600	372.6	100	444	12.6	16.3	414

4.6 Parametric study

The effect of each parameter on the final state is given in Table 5 and Fig. 8. The modulus of the bearing stratum had the largest effect. Between 30 and 240 MPa the dragload rose from 375 to 635 kN, the neutral plane dropped from 11.5 to 15.0 m and the head settlement fell from 22.9 to 8.0 mm. A stiff toe keeps the pile from following the ground, so more of the shaft is dragged.

Interface strength scaled the dragload without moving the neutral plane. An interface factor of 0.70 lowered the dragload by 18%, to 362 kN, with the neutral plane still at 12.7 m.

A larger head load reduced the dragload. With 300 kN the dragload was 511 kN and the neutral plane lay at 13.5 m; with 900 kN, 388 kN and 11.7 m. The maximum axial force still grew with the head load, from 811 to 1288 kN, but only by about 480 kN for the 600 kN added at the head.

The elastic slip of the interface, a numerical parameter that stands for the movement needed to mobilise friction, shifted the dragload from 462 kN at 1 mm to 404 kN at 5 mm. Placing the yield surface with Jaky's coefficient reduced the ground settlement from 373 to 298 mm and the dragload only from 444 to 434 kN.

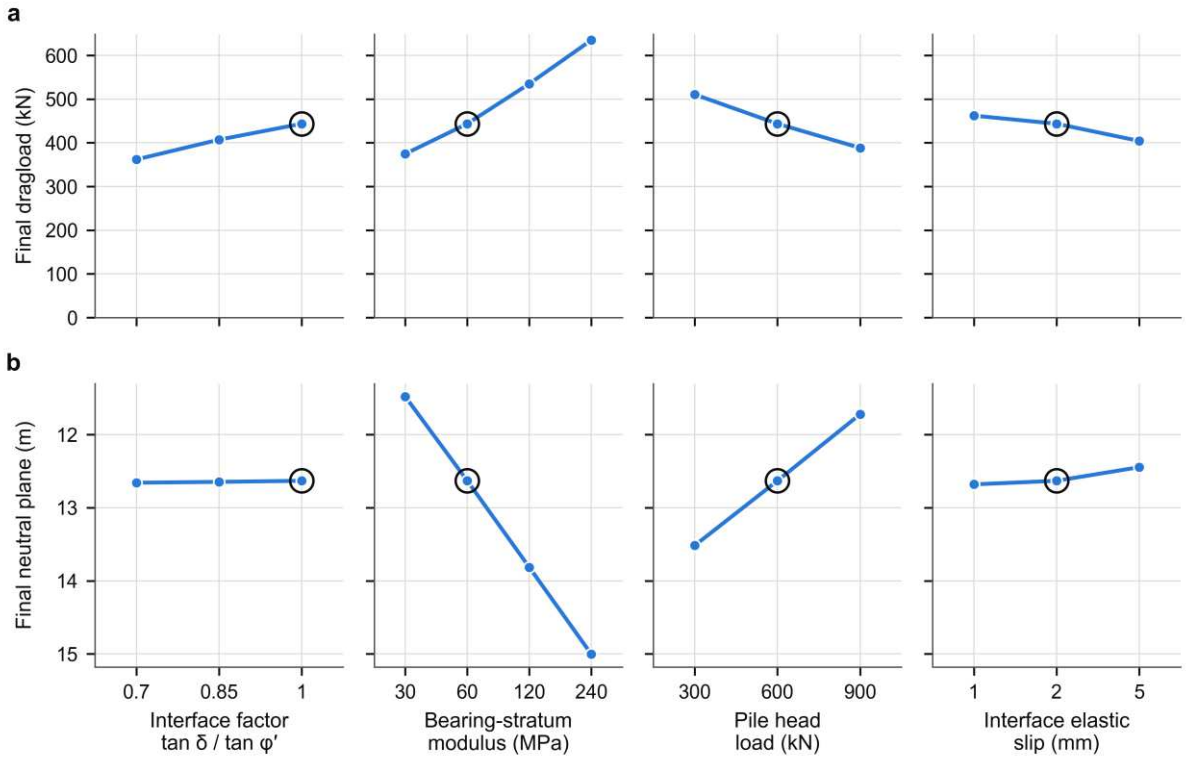


Fig. 8 Effect of four parameters on the final state of the Modified Cam Clay model: **a** dragload; **b** neutral plane depth. The ring marks the base case

Table 5 Parametric study with the Modified Cam Clay model: final state

Variation	Dragload (kN)	Neutral plane (m)	Head settlement (mm)	Time to 90% of dragload (years)
Base case	444	12.63	16.3	171
Interface factor 0.70	362	12.66	16.1	178
Interface factor 0.85	407	12.65	16.2	174
Bearing stratum, E = 30 MPa	375	11.48	22.9	149
Bearing stratum, E = 120 MPa	535	13.81	11.5	175
Bearing stratum, E = 240 MPa	635	15.00	8.0	169
Head load 300 kN	511	13.52	13.2	167
Head load 900 kN	388	11.72	19.7	162
Interface elastic slip 1 mm	462	12.68	16.2	171
Interface elastic slip 5 mm	404	12.45	16.7	167
Drained bearing stratum	414	12.72	15.9	27
Clay permeability × 3	444	12.63	16.3	59
Yield surface placed with Jaky's $K_{0,nc}$	434	12.59	15.9	135

5 Discussion

5.1 Why the rigid-plastic method overestimates the dragload

The unified method is built on a displacement argument, the equality of pile and soil settlement at the neutral plane in Eq. (6), but it converts that argument into forces with a strength rule, Eq. (3), that ignores displacement. The coupled model shows the cost. Shaft shear needs relative movement, and in a continuum that movement has two parts: slip at the interface and shear distortion of the soil around the shaft, which grows with the shear stress and with the inverse of the soil stiffness [43]. In the CH layer the ground settles tens to hundreds of millimetres more than the pile, and both parts are easily supplied. In the CL layer the free-field settlement is only 24 mm at its top, while the pile settles about 15 mm at that depth. The few millimetres left are not enough to mobilise an interface strength of 50 to 60 kPa, so the shear stays well below its limit for several metres on either side of the neutral plane.

This agrees with the numerical evidence that slip controls the dragload and that design methods overpredict it for single piles [20, 21]. It does not contradict the field observation that small movements mobilise shaft shear [4]. What changes from one case to another is how the movement available near the neutral plane compares with the movement required, and in a stiff lower layer the available movement is small. The length of the transition zone therefore depends on the case. It will be short where a soft layer extends to the neutral plane and long where, as here, the neutral plane falls in a stiffer layer.

For design the consequence is uneven. The dragload matters for the structural check of the pile section, and there the unified method errs on the safe side. The neutral plane matters for the settlement of the pile, and there the method performed well once its inputs were consistent with the ground.

5.2 Toe stiffness

Almost half of the difference between the two analyses came from one input, the toe stiffness, and the parametric study ranked the modulus of the bearing stratum above every other parameter. A stiffer toe lowers the neutral

plane and raises the dragload while it reduces the settlement, which is the trade-off behind the advice to found piles in ground that does not settle [13]. In practice the toe load–movement response cannot be left as a default. It deserves the same attention as the compressibility of the clay, through a static loading test with toe instrumentation or a justified load-transfer curve.

5.3 Timing of the dragload

For a structure next to an embankment, the time at which the dragload develops matters as much as its final value. Two results bear on it. The first is that, where the clay can only drain upward, the dragload lags the settlement of the ground. A settlement record under the embankment then gives an upper estimate of how far the dragload has progressed. The second is that this no longer holds if the bearing stratum drains: the dragload then runs ahead of the settlement. The lower clay consolidates early, and although it contributes little settlement, it is the layer that holds the neutral plane and the largest interface strength. In the case analysed, 61% of the dragload was present one year after filling with a pervious stratum. Without it, the same share took more than 50 years. A site investigation for an abutment on piles should therefore establish whether the bearing stratum can drain, which is not a question usually asked of it.

A larger sustained load reduced the dragload, as centrifuge tests and earlier analyses of pile-head load have shown [9, 25, 26]. The two therefore do not simply add in the structural check. The final neutral plane, at 0.70 to 0.75 of the pile length, is also close to the three-quarters of the embedded length reported from centrifuge tests on floating piles [9].

5.4 Limitations

The study is numerical and its parameters are illustrative. It has not been compared with an instrumented pile, and that comparison is the necessary next step. The surcharge is uniform and the pile is single, so lateral soil movement near an embankment slope and group effects [20, 22] are not represented. The pile is wished in place, without the stress changes caused by boring or driving [30]. Strains are small, although the ground settles 0.36 m relative to the pile head. Permeability is constant and secondary compression is ignored, so the times reported are no more than the consequence of the values adopted. Modified Cam Clay with M derived from φ' gives a higher K_0 in normal compression than Jaky's expression, 0.90 from Eq. (13) against 0.76 in the CH layer. The interface strength of that layer is therefore 406 kN where Eq. (3) gives 377 kN. The friction angle adopted for that layer, 14°, is low; it was kept so that both methods used the same input. Finally, the mesh was limited to 1000 nodes by the software edition used; the sensitivity found was small, but the analyses should be repeated with a finer mesh under a full licence.

6 Conclusions

A pile beneath an approach embankment on a high-plasticity clay over a low-plasticity clay was analysed with the unified method and with a coupled consolidation model. For this case:

1. The coupled model gave a final dragload of 444 kN with Modified Cam Clay and 459 kN with an equivalent elastic clay, against 801 kN from the unified method. The neutral plane was at 12.6 and 13.5 m instead of 14.25 m.

2. The difference had two causes of similar weight. The toe stiffness assumed in the unified method was more than twice that of the modelled bearing stratum, which explained 166 kN. Partial mobilisation of shaft shear over a transition zone more than 9 m long explained 180 kN.

3. With inputs consistent with the model, the rigid-plastic method located the neutral plane within about 0.2 m and overestimated the dragload by 32 to 41%. It is a safe estimate for the structural check and a reasonable one for settlement.

4. With drainage towards the surface only, dragload developed later than settlement. With 34% of the settlement complete the pile carried 19% of its final dragload. The relation between the two did not change when the permeability was tripled.

5. Drainage of the bearing stratum controlled the timing. With a pervious stratum 61% of the dragload was present one year after filling; with an impervious one, 4%.

6. Among the parameters varied, the stiffness of the bearing stratum had the largest effect on dragload and neutral plane, followed by head load and interface strength.

These conclusions rest on illustrative parameters and on a single pile under a wide, uniform fill. They should be checked against an instrumented pile before being applied to a project.

Data availability

The input files, scripts and extracted results that support this study are available from the corresponding author on reasonable request.

References

1. Bozozuk, M.: Downdrag measurements on a 160-ft floating pipe test pile in marine clay. Can. Geotech. J. 9(2), 127–136 (1972). https://doi.org/10.1139/t72-014

2. Fellenius, B.H.: Down-drag on piles in clay due to negative skin friction. Can. Geotech. J. 9(4), 323–337 (1972). https://doi.org/10.1139/t72-037

3. Indraratna, B., Balasubramaniam, A.S., Phamvan, P., Wong, Y.K.: Development of negative skin friction on driven piles in soft Bangkok clay. Can. Geotech. J. 29(3), 393–404 (1992). https://doi.org/10.1139/t92-044

4. Fellenius, B.H.: Results from long-term measurement in piles of drag load and downdrag. Can. Geotech. J. 43(4), 409–430 (2006). https://doi.org/10.1139/t06-009

5. Olson, S.J.: Eisenhower Bridge north abutment and approach settlement: a case history of timber pile downdrag and comparative downdrag effect on steel piles. In: Geo-Congress 2020, pp. 119–127. American Society of Civil Engineers, Reston (2020). https://doi.org/10.1061/9780784482841.009

6. Long, J.H., Olson, S.M., Stark, T.D., Samara, E.A.: Differential movement at embankment-bridge structure interface in Illinois. Transp. Res. Rec. 1633(1), 53–60 (1998). https://doi.org/10.3141/1633-07

7. Chalajour, S., Blatz, J.A.: Prediction of drag force on piles subjected to negative skin friction induced by bridge embankment construction based on measured field data. Transp. Geotech. 51, 101507 (2025). https://doi.org/10.1016/j.trgeo.2025.101507

8. Leung, C.F., Liao, B.K., Chow, Y.K., Shen, R.F., Kog, Y.C.: Behavior of pile subject to negative skin friction and axial load. Soils Found. 44(6), 17–26 (2004). https://doi.org/10.3208/sandf.44.6_17

9. Lam, S.Y., Ng, C.W.W., Leung, C.F., Chan, S.H.: Centrifuge and numerical modeling of axial load effects on piles in consolidating ground. Can. Geotech. J. 46(1), 10–24 (2009). https://doi.org/10.1139/T08-095

10. Li, B., Yu, J.F.: Bearing capacity of piles with negative skin friction based on field tests. Results Eng. 28, 108320 (2025). https://doi.org/10.1016/j.rineng.2025.108320

11. Fellenius, B.H.: Unified design of piled foundations with emphasis on settlement analysis. In: Current Practices and Future Trends in Deep Foundations, pp. 253–275. American Society of Civil Engineers, Reston (2004). https://doi.org/10.1061/40743(142)15

12. Coffman, R.A., Blanchard, J.D., Stuedlein, A.W., Jana, A., Budge, A.: Design of Piles for Downdrag. NCHRP Research Report 1112. National Academies Press, Washington (2024). https://doi.org/10.17226/27863

13. Poulos, H.G.: A practical design approach for piles with negative friction. Proc. Inst. Civ. Eng. Geotech. Eng. 161(1), 19–27 (2008). https://doi.org/10.1680/geng.2008.161.1.19

14. Alonso, E.E., Josa, A., Ledesma, A.: Negative skin friction on piles: a simplified analysis and prediction procedure. Géotechnique 34(3), 341–357 (1984). https://doi.org/10.1680/geot.1984.34.3.341

15. Matyas, E.L., Santamarina, J.C.: Negative skin friction and the neutral plane. Can. Geotech. J. 31(4), 591–597 (1994). https://doi.org/10.1139/t94-069

16. Wong, K.S., Teh, C.I.: Negative skin friction on piles in layered soil deposits. J. Geotech. Eng. 121(6), 457–465 (1995). https://doi.org/10.1061/(ASCE)0733-9410(1995)121:6(457)

17. Kim, H.J., Mission, J.L.C.: Development of negative skin friction on single piles: uncoupled analysis based on nonlinear consolidation theory with finite strain and the load-transfer method. Can. Geotech. J. 48(6), 905–914 (2011). https://doi.org/10.1139/t11-004

18. Cao, W., Chen, Y., Wolfe, W.E.: New load transfer hyperbolic model for pile-soil interface and negative skin friction on single piles embedded in soft soils. Int. J. Geomech. 14(1), 92–100 (2014). https://doi.org/10.1061/(ASCE)GM.1943-5622.0000289

19. Wu, W., Wang, Z., Zhang, Y., El Naggar, M.H., Wu, T., Wen, M.: Semi-analytical solution for negative skin friction development on deep foundations in coastal reclamation areas. Int. J. Mech. Sci. 241, 107981 (2023). https://doi.org/10.1016/j.ijmecsci.2022.107981

20. Lee, C.J., Bolton, M.D., Al-Tabbaa, A.: Numerical modelling of group effects on the distribution of dragloads in pile foundations. Géotechnique 52(5), 325–335 (2002). https://doi.org/10.1680/geot.2002.52.5.325

21. Jeong, S., Lee, J., Lee, C.J.: Slip effect at the pile–soil interface on dragload. Comput. Geotech. 31(2), 115–126 (2004). https://doi.org/10.1016/j.compgeo.2004.01.009

22. Lee, C.J., Ng, C.W.W.: Development of downdrag on piles and pile groups in consolidating soil. J. Geotech. Geoenviron. Eng. 130(9), 905–914 (2004). https://doi.org/10.1061/(ASCE)1090-0241(2004)130:9(905)

23. Comodromos, E.M., Bareka, S.V.: Evaluation of negative skin friction effects in pile foundations using 3D nonlinear analysis. Comput. Geotech. 32(3), 210–221 (2005). https://doi.org/10.1016/j.compgeo.2005.01.006

24. Hanna, A.M., Sharif, A.: Drag force on single piles in clay subjected to surcharge loading. Int. J. Geomech. 6(2), 89–96 (2006). https://doi.org/10.1061/(ASCE)1532-3641(2006)6:2(89)

25. Chen, R.P., Zhou, W.H., Chen, Y.M.: Influences of soil consolidation and pile load on the development of negative skin friction of a pile. Comput. Geotech. 36(8), 1265–1271 (2009). https://doi.org/10.1016/j.compgeo.2009.05.011

26. Chiou, J.-S., Wei, W.-T.: Numerical investigation of pile-head load effects on the negative skin friction development of a single pile in consolidating ground. Acta Geotech. 16(6), 1867–1878 (2021). https://doi.org/10.1007/s11440-020-01134-0

27. Yan, W.M., Sun, T.K., Tham, L.G.: Coupled-consolidation modeling of a pile in consolidating ground. J. Geotech. Geoenviron. Eng. 138(7), 789–798 (2012). https://doi.org/10.1061/(ASCE)GT.1943-5606.0000651

28. Sun, T.K., Yan, W.M., Su, D.: Fully coupled consolidation analysis of shear strength mobilization and dragload of a pile subject to negative skin friction. Int. J. Geomech. 15(3), 04014057 (2015). https://doi.org/10.1061/(ASCE)GM.1943-5622.0000381

29. Wu, Y., Ren, Y., Liu, J., Ma, L.: Analysis of negative skin friction on a single pile based on the effective stress method and the finite element method. Appl. Sci. 12(9), 4125 (2022). https://doi.org/10.3390/app12094125

30. Koch, M.C., Chand, B., Mukherjee, M., Dey, A.: Generation of negative skin friction and drag load in near-offshore pile foundations: a numerical study addressing pile installation effects. Ocean Eng. 340, 122219 (2025). https://doi.org/10.1016/j.oceaneng.2025.122219

31. Mohsen, A.H., Albusoda, B.S.: An experimental study evaluating the negative skin friction on single and group of close-ended circular pipe piles embedded in gypseous soil. Transp. Infrastruct. Geotech. 11(4), 1903–1927 (2024). https://doi.org/10.1007/s40515-023-00349-4

32. Abdulwadood, H.W., Albusoda, B.S.: Experimental observation of negative skin friction performance on different geometries of floating piles in gypseous soil. Transp. Infrastruct. Geotech. 13(5), 153 (2026). https://doi.org/10.1007/s40515-026-00912-9

33. Liu, K., Chen, J., Kang, J.: Long-term consolidation settlement behavior of piled raft foundations on soft clay considering strain rate effect. Transp. Infrastruct. Geotech. 12(7), 242 (2025). https://doi.org/10.1007/s40515-025-00702-9

34. Pham, V.-N., Trinh, H., Phan, H.-N., Ho, M.-H., Le, D.-V., Oh, E.: Automated finite element modeling and predictive assessment of deformation in HSR bridge–embankment transition zones on soft soil. Transp. Infrastruct. Geotech. 13(6), 232 (2026). https://doi.org/10.1007/s40515-026-01004-4

35. Sengupta, I., Chowdhury, S.: A numerical investigation of time-dependent behavior of geosynthetic-reinforced pile-supported embankments. Transp. Infrastruct. Geotech. 13(7), 255 (2026). https://doi.org/10.1007/s40515-026-01015-1

36. Wood, D.M.: Soil Behaviour and Critical State Soil Mechanics. Cambridge University Press, Cambridge (1991). https://doi.org/10.1017/CBO9781139878272

37. Meyerhof, G.G.: Bearing capacity and settlement of pile foundations. J. Geotech. Eng. Div. 102(3), 197–228 (1976). https://doi.org/10.1061/AJGEB6.0000243

38. Mayne, P.W., Kulhawy, F.H.: K0–OCR relationships in soil. J. Geotech. Eng. Div. 108(6), 851–872 (1982). https://doi.org/10.1061/AJGEB6.0001306

39. Biot, M.A.: General theory of three-dimensional consolidation. J. Appl. Phys. 12(2), 155–164 (1941). https://doi.org/10.1063/1.1712886

40. Terzaghi, K.: Theoretical Soil Mechanics. Wiley, New York (1943). https://doi.org/10.1002/9780470172766

41. Vermeer, P.A., Verruijt, A.: An accuracy condition for consolidation by finite elements. Int. J. Numer. Anal. Methods Geomech. 5(1), 1–14 (1981). https://doi.org/10.1002/nag.1610050103

42. Potyondy, J.G.: Skin friction between various soils and construction materials. Géotechnique 11(4), 339–353 (1961). https://doi.org/10.1680/geot.1961.11.4.339

43. Randolph, M.F., Wroth, C.P.: Analysis of deformation of vertically loaded piles. J. Geotech. Eng. Div. 104(12), 1465–1488 (1978). https://doi.org/10.1061/AJGEB6.0000729